The International Journal of Engineering and Science (IJES)
|| Volume || 8 || Issue || 8 Series I || Pages || PP 07-14|| 2019 ||
ISSN (e): 2319 – 1813 ISSN (p): 23-19 – 1805

Optimization under Uncertainties of a Valveless Diaphragm Pump using the Cut-Cell Method

D. Kapsoulis, K. Samouchos, X. Trompoukis and K. Giannakoglou
[1]*National Technical University of Athens, School Mech. Eng., Parallel CFD & Optimization Unit, Athens15780, Greece*
Corresponding Author:D. Kapsoulis

----------ABSTRACT----------
In the absence of valves, diaphragm pumps equipped with a moving diaphragm to generate the unsteady flow in the right direction are designed to deliver the maximum or the required volume flowrate while reducing/suppressing backflow. Operating and manufacturing uncertainties affect the performance of pumps, such asthe micropump this paper is dealing with, and should be taken into consideration during the designloop. This paper presents such a design-optimization by incorporating (a) the cut-cell method for the CFD analysis of the unsteady flow, (b) the non-intrusive polynomial chaos expansion method, supportedby aSmolyaksparse grid, to quantify uncertainties in the performance metrics, (c) a Pareto front seeking evolutionary algorithm with some add-ons to reduce the otherwise excessive CPU cost and (d) an intercalary gradient-based improvement of selected individuals, assisted by the continuous adjoint method to compute the gradient of the objective functions, running regularly within the evolutionary optimization. Overall, this paper extends a previous optimization of the same diaphragm micropump, that time in the absence of uncertainties.
KEYWORDS: *Diaphragm micropump, Cut-cell method, Uncertainty quantifications, Hybrid optimization, Evolutionary algorithms, Gradient-based optimization, Adjoint method.*

Date of Submission: 28-07-2019 Date of acceptance: 10-08-2019

I. INTRODUCTION

Diaphragm pumps can efficiently andnoiselessly pump various types of fluids; they deliver a time-varying flowrate which can occasionally become more uniform byoperating more than one pumps in parallel,[1]. Depending on their size, important differences may exist. Large diaphragm pumps, often used for cleaning tanks or pumping sewage, are equipped with inlet/outlet valves to avoid backflow. Micropumps, mostly used as medical analysis devices andfor biochemical-processing applications[2][13], rarely bring valves due to their reduced lifetime and the damage or, at least, the extra resistance to sensitive fluids [7].In the absence of valves, their main components are the inlet and outlet ducts (two diffusers in our case), a chamber and a periodically moving diaphragm determining their pumping capabilities.

This paper focuses on the design of an optimal 3D valveless diaphragm micropump, in the presence of uncertainties associated with the motion of the diaphragm. The optimization is carried out using a parameterization scheme for the diaphragm motion,introducing eightdesign (also, uncertain) variables in total.For the analysis of the 3D viscous flow, an in-house CFD solver based on the cut-cell method [4],a variant of the general class of Immersed Boundary Methods (IBM), is used.The cut-cell method uses a Cartesian grid that remains stationary during the diaphragm motion, by covering and uncovering grid cells, beingautomatically refined close to the moving geometry and de-refined elsewhere.

Two performance metrics related to the quality of the flow at the exit of the pump are introduced: the net flowrate andthe backflow, both measured at the exit of the second diffuser.Two objective functions are built by combining the first two statistical moments of these twometrics.With these two objectives, to be minimized/maximized, the Pareto front of non-dominated solutions is computed using an Evolutionary Algorithm (EA).EAs can reach global optimal solutions but might need an excessive number of calls to the CFD tool. The cost can be reducedthrough the implementation of surrogate models or metamodels (Metamodel-Assisted EA or MAEA) and the Principal Component Analysis (PCA) of the population members.Metamodels replicate the objective functions computed by the CFD tool, at an almost negligible computational cost.The PCA transforms the design space into a new feature space, in which the evolution operators perform much better; thisalso assists metamodels to be trained with significant input variables only, as identified by the PCA.

In this paper, the MAEA (being the background optimization tool) isselectively assisted by gradient-based (GB)improvements, giving rise to a hybrid algorithm, [5][10], in whichthe EAundertakes the exploration of the design space and the GB method the refinement of selected promising solutions.In this paper, the GB method is assisted by the continuous adjoint approach computing the requiredgradients at practically the cost of an extra CFD evaluation, independent of the number of design variables.

Operating and manufacturing uncertainties affect the performance of the pump and must beaccounted for during the design-optimization.Alldesign variables are considered as uncertain (stochastic) variables.By computing mean valuesand standard deviations of the two performance metrics and forming their weighted sum, the two objective functions of the optimization under uncertainties arise.In this paper, the non-intrusive Polynomial Chaos Expansion (PCE) [3]is used to compute the required statistical moments.The Gauss integration rules determine a set of Gaussian nodes, corresponding to specific data-sets of the stochastic variables, and each node is an operation mode to be evaluated on the CFD solver. The overall number of Gaussian nodes and, thus, the computational costare reduced by using the Smolyak sparse grid theory[11].

This paper extends the work presented in[4], in which the diaphragm motion of the same micropump is optimized for maximum net flowrate and minimum backflow without though taking operating or manufacturing uncertaintiesinto account. At the end of the work presented in [4], the uncertainty quantification (UQ) of just a few of the computed optimal

solutions was performed, showing that operating uncertainties strongly affect the performance of the micropump.With the previous message in mind, we take a step forward by including uncertainties within the optimization loop.

.

II. PARAMETERIZED PUMP AND PERFORMANCE METRICS

The diaphragm pump to be designed has a $\sim 9\text{mm}$ long shape with an overall volume, prior to deforming the diaphragm, equal to $\sim 40\ \text{mm}^3$. This chamber brings two identical straight diffusers with a 0.20/0.03 ratio of the outlet and inlet cross-sections. The top face of the chamber (size $L_x \times L_z$; located at $y = 0$) is mostly covered by the moving diaphragm.This diaphragm covers only the $b_1 L_x \times b_2 L_z$ central part of the rectangularface, withb_1 and b_2 being the first two design variables. The diaphragm undergoes a periodic motion with a constant period $T = 0.02\text{sec}$. There are six more design variables (b_3 ... b_8)parameterizingits motion. Assuming that, at each instant $t \in [0, T]$, $y_{max} \geq 0$ is the maximum immersion of the diaphragm, this is given by

$$y_{max} = b_3 \exp\left(-b_4\left(t - \frac{T}{2}\right)^2\right)\left(1 - \left|1 - \frac{2t}{T}\right|\right)$$

which involvesb_3(directlyaffecting the maximum immersion) and b_4 (controlling how steep this distribution is). Thelongitudinal location of the maximum immersion, at each instant (t), is given by $x/L_x^m = t/T$, where $L_x^m = b_1 L_x$. The longitudinal deformation y(x) of the diaphragm along the symmetry plane is given by polynomial expressions, involving two more design variables, namely b_5 and b_6.Finally, the last two design variables, b_7 and b_8, determine the span-wise immersion'spolynomial distribution y(z). The interested reader may find the detailed parameterization scheme in [9]and a sketch of an arbitrary diaphragm motion in Figure 1.

The two performance metrics characterizing the operation of the diaphragm pump, namely the net volume flowrate (Q_2) and the backflow (Q_1) are defined by

$$Q_{net} = \frac{6 \cdot 10^{10}}{T} \int_T \int_{S_{outlet}} \vec{V}(t) \cdot \vec{n}\, dS dt \ (\mu l/min)$$

and

$$Q_{bf} = \frac{6 \cdot 10^{10}}{T} \int_T \int_{S_{outlet}} \min(0, \vec{V}(t)) \cdot \vec{n}\, dS dt \ (\mu l/min)$$

where $\vec{V}(t)$ is the velocity vector and$\vec{n}$ the outward unit normal vector; quantities on the r.h.s. of the above formulas are in SI units.

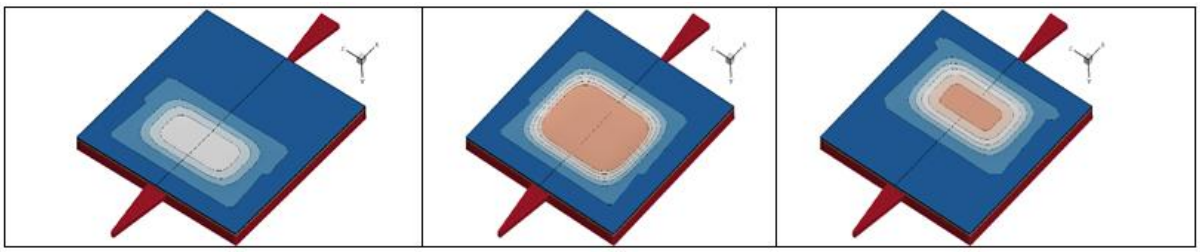

Figure 1 Perspective view of the valveless diaphragm micropump. Fluid flows from left-bottom to right-top. Diaphragm deformations at 30% (left), 50% (m) and 70% (right) of the period, respectively.

III. FLOW EQUATIONS & THE CUT-CELL METHOD

The Navier-Stokes equations, governing the 3D unsteady viscous flow of an incompressible fluid, read

$$\Gamma_{nm}^{-1} \frac{\partial V_m}{\partial \tau} + \frac{\partial U_n}{\partial t} + \frac{\partial f_{nk}^{inv}}{\partial x_k} - \frac{\partial f_{nk}^{vis}}{\partial x_k} = 0$$

Equation 1

The above equation includes the (real) time (t) derivative of $\vec{U} = [0\ u_1 u_2 u_3]^T$ and the pseudo-time (τ) derivative of $\vec{V} = [p\ u_1 u_2 u_3]^T$, where p is the pressure divided by the constant fluid's density and u_1, u_2, u_3 are the Cartesian components of fluid's velocity. The preconditioning matrix Γ^{-1} depends on the constant artificial speed of sound β, [9]. $\vec{f}^{inv}$, $\vec{f}^{vis}$ are the inviscid and viscous fluxes, respectively.

In the cut-cell method, grid generation starts from a single "large" cell covering the entire flow domain. This "large"cell is decomposed again and again, though successive subdivisions of each cell into eight sub-cells, and cells intersecting the flow domain boundaries are additionally refined; the termination criterion is the user-defined minimum allowed cell size. The use of an octree data structure makes this procedure quite fast, with low memory requirements. While computing the intersection of cells with the boundaries, cells or parts of them which do not belong to the fluid domain are neglected and the flow equations are solved within the remaining cells. Thougheach cell is restricted to have at most four neighboring cells per face, small cut-cells may be next to much bigger ones.This may introduceflow prediction errors and, to avoid them,adjacent small and bigger cells merge to form hyper cells. In specific, each small cell is paired/merged with the neighboring cell with volume higher than a user-defined threshold that shares the largest face with it. Should this criterion fail, the neighboring cell with the largest volume is chosen. The algorithm allows a hyper finite volume to be formed by more than one cells.

The governing equations are discretized using second-order accuracy, according to the cell-centered finite-volume method, while taking thegeometrical conservation law into consideration. At each time-instant the grid is de-refined or

refined in areas far from and close to the moving diaphragm, respectively. As the diaphragm moves, cells change in shape or migrate from the fluid to the solid region and vice-versa. An upwind scheme is used for the convection terms.

IV. UNCERTAINTY QUANTIFICATION

For the UQ of the micropump's performance in the presence of uncertainties, the two performance metrics are considered as stochastic functions ($Q_1 = Q_{bf}$ & $Q_2 = Q_{net}$) in terms of the stochastic (herein, coinciding with the design) variables b_k, by associating user-defined probability density functions (PDFs) with them. In this paper, all uncertain variables follownormal distributions. So, Hermite Polynomials $He_j(\vec{b})$, with j defining the maximum degree of each of them, are used to express the stochastic function Q_i by the truncated term [3],

$$Q_i(\vec{b}) \approx \sum_{j=1}^{q} a_{i,j} He_j(\vec{b})$$

where q is the user-defined chaos order and$a_{i,j}$ are the PCE coefficients.The first two statistical moments of Q_i (mean values$\hat{\mu}_{Q_i}$and variances$\hat{\sigma}^2_{Q_i}$) are computed throughGalerkin projections as

$$\hat{\mu}_{Q_i} = a_{i,0}, \quad \hat{\sigma}^2_{Q_i} = \sum_{j=1}^{q} a^2_{i,j}$$

with

$$a_{i,j} = \int_S Q_i(\vec{b})\, He_j(\vec{b}) PDF(\vec{b}) d\vec{b} = \sum_{m=1}^{M} r_m Q_i(\vec{p}_m), \quad j = 0,1,\dots,q$$

Equation 2

where S is the objective space and r_m are known weights. The M Gaussian nodes$\vec{p}_m$within the domain of integration and the$r_m$values are determined by the Gauss quadrature integration rules, in this case with the use ofSmolyak sparse grid, for the reasons explained in thesectionVI. For each set of design vectors (candidate solution) and each objective, the first two statistical moments are computed at the cost of M calls to the CFD software.

The derivatives of the first two statistical momentsof Q_1 and Q_2w.r.t the design variables $\vec{b}$(required for the GB improvement) are derived by differentiatingEquation 2w.r.t.b_k

$$\frac{\delta a_{i,j}}{\delta b_k} = \int_S \frac{\delta Q_i}{\delta b_k}(\vec{b}) He_j(\vec{b}) PDF(\vec{b}) d\vec{b}, \quad i = 1,2, \quad j = 0,1,\dots,q$$

Equation 3

where the derivatives $\frac{\delta Q_i}{\delta b_k}$ are computed by the continuous adjoint method. Then, the derivatives of the mean values and standard deviations are computedas

$$\frac{\delta \hat{\mu}_{Q_i}}{\delta b_k} = \frac{\delta a_{i,0}}{\delta b_k}, \qquad \frac{\delta \hat{\sigma}_{Q_i}}{\delta b_k} = \frac{1}{\hat{\sigma}_{Q_i}} \sum_{j=1}^{q} a_{i,j} \frac{\delta a_i}{\delta b_k}$$

The computation of$\frac{\delta F_i}{\delta b_k}(F_i, i = 1,2$ are the two optimization objectives to be defined in the sectionVI) is then straightforward.

V. THE HYBRID OPTIMIZATION METHOD

The optimization method involves gradient-free and gradient-based search.The background tool is a MAEA which computes the Pareto front of non-dominated solutionsby performing a small percentage of the calls to the (computationally expensive) CFD software required otherwise;this is achieved not only by implementing on-line trained metamodels but, also, through the PCA of the evolving populations,in each generation.Next to the MAEA, an adjoint-based (GB) improvement of some of the current non-dominated solutions is implemented.

1. ThePCA-drivenMAEA

The PCA-driven MAEA used in this paper is based on a (μ,λ) EA with real encoding; μ and λ stand for the parent and offspring population sizes. During the evolution, a database (DB) records all candidate solutions evaluated on the CFD software and there is also an elite set (with e members at most) of the best-so-far solutions. The use of on-line trained metamodels starts after a few (a user-defined small number) generations, during which a minimum number of evaluated individuals is stored into the DB. In all subsequent generations, the λ offspring are first evaluated on metamodels trained, on the fly, on a small number of neighboring individuals found in the DB. It is important to mention that a separate metamodel (Radial Basis Function, RBF, network) is trained for each and every individual; the reader should find more on this MAEA for many objective optimization problems in [6]. All offspring are thus pre-evaluated on personalized metamodels, i.e.λ different metamodels should be trained. Then, a few top of them are identified (according to the outcome ofthe approximate pre-evaluation) and re-evaluated on the CFD software. Even without the PCA-based add-on mentioned in the next paragraph, this MAEA reduces the number of calls to the CFD software by even an order of magnitude.

To avoid the MAEA performance degradation in problems with many design variables, the PCA of the current offspring population controls the evolution operators and/or reduces the number of input units used to train the metamodels**Error! Bookmark not defined.**. Population members are first transformed to a new feature space with ordered variances, computed by the Kernel PCA, where evolution operators perform better. In the new space, higher mutation probabilities are assigned to directions with smaller variances. Also, for each offspring, once the training patterns for its "personalized" metamodel have been selected, these are transformed to the feature space (still based on the Kernel PCA) and

the metamodel inputs along the direction with the smaller variances are truncated, as less important. With less input units, the metamodels predict better at lower computational cost.

2. Adjoint Equations and Gradient Computation

The gradient-based counterpart of the hybrid optimization method computes the gradient of the function F to be minimized (herein, F is the weighted sum of the objectives F_1, F_2, as defined later on; the computation of weights is an important part of the hybrid search method that is carried out automatically, see subsection 3) and performs a descent step, indicatively expressed as $b_i^{new} = b_i^{old} - \eta \frac{\delta F}{\delta b_i}|^{old}$, where η is a user-defined step.

The presentation of the mathematical development of the method that computes the gradient, in all detail, is beyond the scope of this paper; the interested reader should refer to [9]. In brief, the continuous adjoint method augments F by the time and space integrals of the governing (flow) equations, multiplied by the adjoint fields Ψ_n. The so-defined augmented F is written as,

$$F_{aug} = F + \int_T \int_{\Omega(t)} \Psi_n R_n d\Omega dt$$

Equation 4

where $\Omega(t)$ is the volume of the instantaneous fluid domain. F_{aug} is equal to F, since the last term on the r.h.s.is zero. Equation 4 is differentiatedw.r.t.b_i and the adjoint variable fields are used to eliminate the variations in the flow variables $\vec{V}$ w.r.t. b_i, the computation of which has a cost that scales with the number of design variables. This gives rise to unsteady adjoint PDEs, which (assuming F to be an integral over the boundaries of the domain; which in this case is our application) are

$$R_m^A = \Gamma_{nm}^{-1} \frac{\partial \Psi_n}{\partial \tau} - \frac{\partial \bar{\Psi}_m}{\partial t} - A_{nmk} \frac{\partial \Psi_n}{\partial x_k} - \frac{\partial f_{km}^{A,vis}}{\partial x_k} = 0$$

Vector$\vec{\bar{\Psi}}$ comprises the adjoint velocities only, i.e. $\vec{\bar{\Psi}} = [0\ \Psi_2 \Psi_3 \Psi_4]^T$,$A_{nmk} = \frac{\partial f_{nk}^{inv}}{\partial V_m}$is the Jacobian of theinviscid fluxes,$f_k^{A,vis} = \left[0\ \tau_{1k}^A \tau_{2k}^A \tau_{3k}^A\right]^T$ is the adjoint viscous flux and $\tau_{km}^A = \nu(\frac{\partial \Psi_{k+1}}{\partial x_m} + \frac{\partial \Psi_{m+1}}{\partial x_k})$are the adjoint viscous stresses.The presentation of the adjoint boundary conditions is omitted in the interest of space. Finally, the expression of the sensitivity derivatives of F is

$$\frac{\delta F}{\delta b_i} = \int_T \int_{S_D} (\Psi_1 n_m - \tau_{km}^A n_k) \left(\frac{\delta u_m^D}{\delta b_i} - \frac{\partial u_m}{\partial x_l} \frac{\delta x_l}{\delta b_i} \right) dS dt$$

Equation 5

where S_D is the diaphragm's surface. In Equation 5, the derivatives of the diaphragm velocity $\left(\frac{\delta u_m^D}{\delta b_i}\right)$and position $\left(\frac{\delta x_l}{\delta b_i}\right)$ are given by closed-form expressions, in terms of time, space and $\vec{b}$,which results from the differentiation of the diaphragm motion.

The two performance metrics used in this paper stand for the backflow at the pump's exit and the net volume of fluid pumped within a period T, respectively, as mentioned in section II. Since function "min" (contained in the definition ofQ_1) cannot be differentiated, asigmoid function

$\mathcal{S}(Q) = 1 - \frac{1}{1+e^{k_2(Q-Q_{crit})+k_1}}$is used instead, with the constants $k_1 = ln\left(\frac{1}{1-f_2} - 1\right)$, $k_2 = \frac{ln\left(\frac{1}{1-f_2}-1\right)-k_1}{Q_{int}-Q_{crit}}$and $Q = -u_k n_k$wheref_1, f_2 are two user-defined constants. Q_1 is thus transformed to a differential function and allows for the development of the continuous adjoint method.Regarding the optimization under uncertainties, derivatives $\frac{\delta a_{i,j}}{\delta b_q}$ are needed as it arises fromEquation 3, meaning that the adjoint equations must be solved for each Gaussian node and each objective. M CFD runs are required per individual evaluation plus$2M$adjoint runs per GB improvement.

3. The Hybrid Optimization Algorithm

The two-objective optimization aims at minimizing $F_1 = \mu_{Q_{bf}} + \sigma_{Q_{bf}}$ while maximizing $F_2 = \mu_{Q_{net}} - \sigma_{Q_{net}}$, as computed using the non-intrusive PCE method, sectionIV. The PCA-driven MAEA of subsection1is the background search method which updates the front of non-dominated solutions. The implementation of the GB method starts by concatenating the two objectives in a single scalar function ($F = \sum_{i=1}^{2} w_i F_i$; to be minimized), using weights that are automatically computed by the method. Then, the adjoint method computes the gradient of F w.r.t.b_i. This gradient is all we need to improve the selected individual by moving them in the steepest descent direction,with a user-defined step value η. The GB improvement could be applied to all non-dominated solutions in each generation, but the cost of computing gradients for all of them makes the method quite expensive. For this reason, GB improvements are applied to just a few automatically selected individuals in each generation. GB improvements startsimultaneously with the metamodels. They are applied to a few individuals (their number is user-defined) generated during the re-evaluation on the CFD model, belonging to the current front of non-dominated solutions. For them, a single descent direction, referred to as the Pareto Advancement Direction (PAD), is computed; the role of $w_i$is to determine the PAD. Its role is to simultaneously improve all objective functions by creating a new individual dominating the processed one. In [5], a technique to "appropriately" compute the PAD has been proposed and briefly repeated below.

The gradient of F is given by$\frac{\delta F}{\delta b_j} = \sum_{i=1}^{2} w_i \frac{\delta F_i}{\delta b_j}$. As said before, the PAD depends on w_i and the PCA technique that converts a data set ($\boldsymbol{D}$)of M observations $\vec{F} \in R^2$, formed by the objective function values of the current front members,into a set of uncorrelated principal components.The PCA computes the covariance matrix **P** of **D** and, then, solves an eigenproblem to define the eigenvalues $\boldsymbol{\Lambda}$ and eigenvectors $\boldsymbol{U}$. Through the following equation $\vec{c} = \vec{c}(\vec{F}) = \boldsymbol{U}(\vec{F} - \vec{\mu})$, $\vec{c} \in R^2$any objective vector $\vec{F}$is mapped onto the so-defined new feature space,where $\vec{\mu}$ is the vector of mean values of the objective functions of $\boldsymbol{D}$.Note that the elements of $\vec{c}$ correspond to directions with variances in descending order.The selected population members are updated by moving them in the direction with the smallest variance,which is considered nearly "perpendicular" to the current front.To do so, the gradients $\frac{\delta F}{\delta b_j}$are mapped onto the feature space, $\frac{\delta \vec{c}}{\delta b_j} = \boldsymbol{U}\frac{\delta \vec{F}}{\delta \mathrm{b_j}}$ which results by differentiating the above equation and the last/second rowof the $\frac{\delta \vec{c}}{\delta \mathrm{b_j}}$ matrix replaces $\frac{\delta \mathrm{F}}{\delta \mathrm{b_j}}$ in the steepest descent equation.

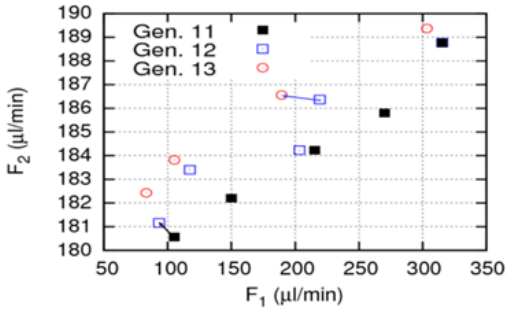

Figure *2*demonstrates the way the GB method updates, between three (arbitrarily selected)successive generations, the front of non-dominated solutions. During almost all generations, the GB method successfully updates at least one individual.

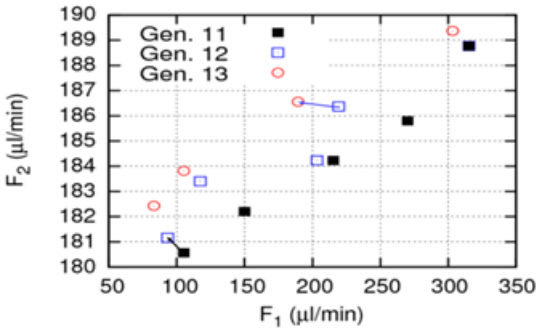

Figure 2 PAD (blue and red arrows) upgrading the fronts of three consecutive generations. Only a part of the front is shown.Points connected by a straight line correspond to intercalary GB improvements.

VI. OPTIMIZATION RESULTS

The optimization under uncertainties performed starts from an existing (reference) micropump that delivers $\mathrm{Q_{net}} = 0.48\ \mu\mathrm{l/min}$ of fluid witha non-negligible backflow rate ($\mathrm{Q_{bf}} = 0.06\mu\mathrm{l/min}$).Therefore, it was decided to run a two-objective optimizationaiming at minimum $\mathrm{F_1} = \mu_{\mathrm{Q_{bf}}} + \sigma_{\mathrm{Q_{bf}}}$(regarding$\mathrm{Q_{bf}}$) andmaximum$\mathrm{F_2} = \mu_{\mathrm{Q_{net}}} - \sigma_{\mathrm{Q_{net}}}$ (regarding $\mathrm{Q_{net}}$), as already explained above.All mean values, standard deviations and objective functions are measured in $\mu\mathrm{l/min}$.The PCA-driven MAEA is setup with $\mu = 6$, $\lambda = 12$ andmetamodels and the PCA technique are activated just after the first generation.The GB improvement updates only one individual per generation, by performing a single descent step;the required gradients are computed by the continuous adjoint method.

For the optimization, lower and upper bounds for the eight design variables have been defined. Since all design variables are also considered as normally distributed uncertain variables, these bounds are practically associated with their mean values.Their standard deviationis set to reasonably small values for each design variable.Working with the non-intrusive PCE, with 8 stochastic variables and chaos order equal to one, a great number of CFD-based evaluations (256, in such a case; to compute 9 expansion coefficients) per candidate solution is required. To avoid this high cost, a Smolyaksparse grid [11]is implemented;at the cost of17 evaluationson the cut-cell software, the same coefficients are approximated.Thus, each individual's evaluation costs 17 CFD runs and, if selected for GB refinement, another2×17adjoint runs are needed to compute the gradients.

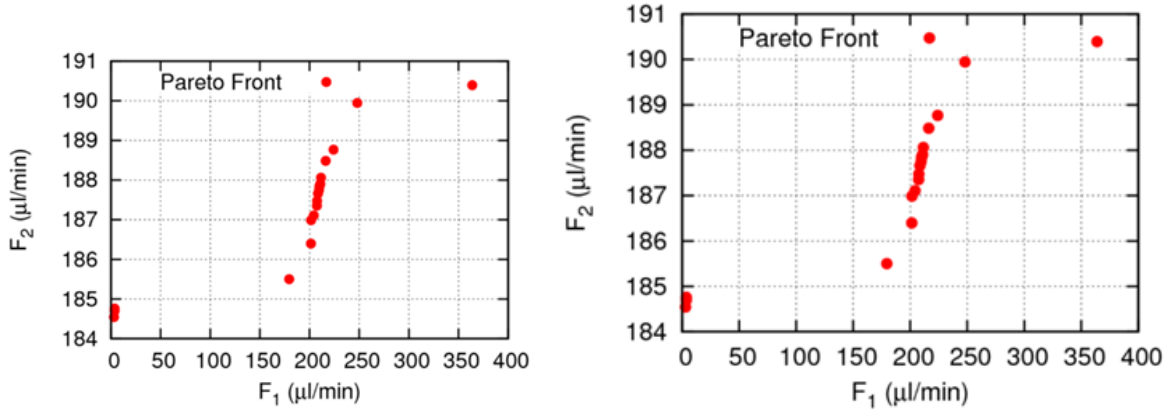

Figure ***3***shows the computed front of non-dominated solutions achieved after the equivalent cost of1400 CFD runs. Moreover, the design variables for the two front edges along with the reference solution are presented in the parallel coordinates diagram shown in

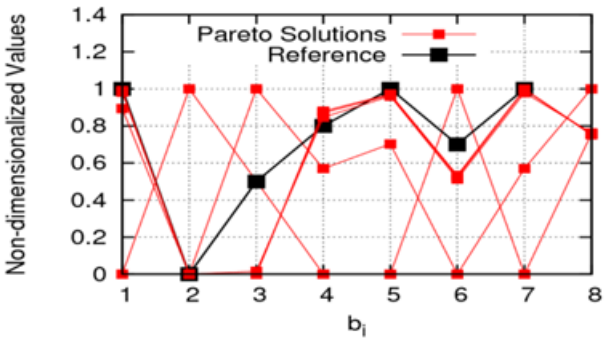

Figure ***4***.

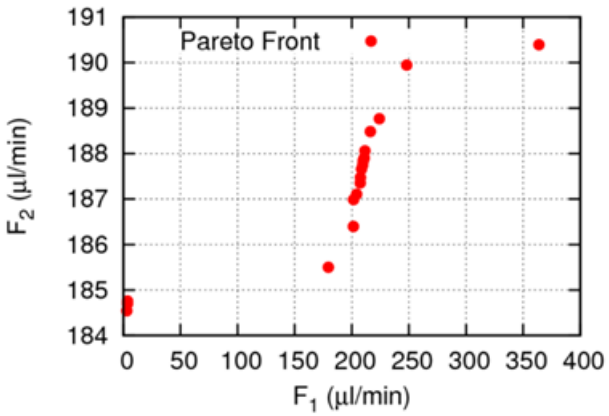

Figure 3 The computed Pareto front of non-dominated solutions.

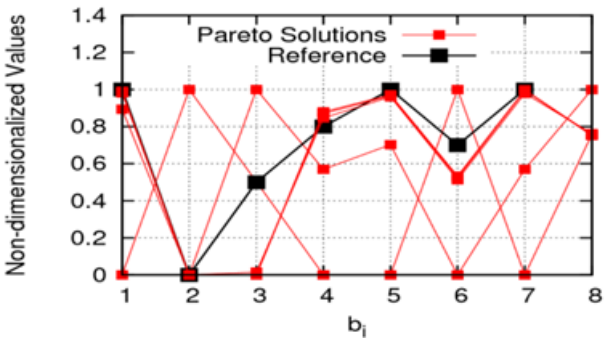

Figure 4 Parallel Coordinates of the two front edges (in red) and the reference solution (in black).

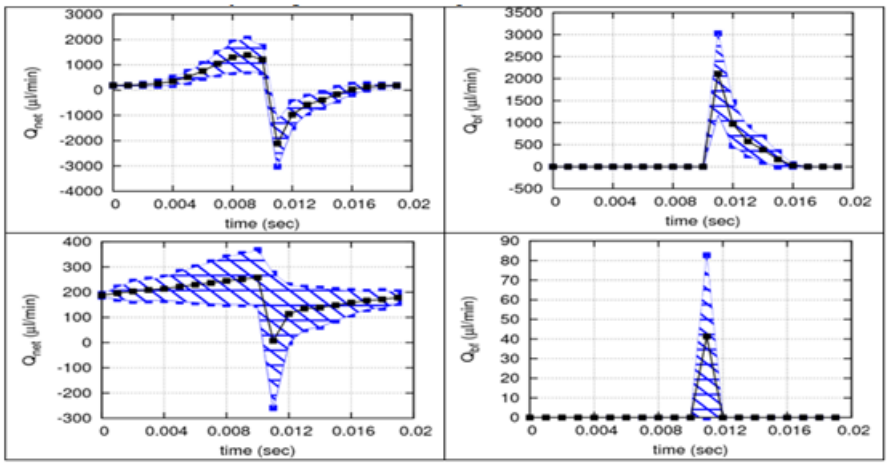

Figure *5* shows how the backflow and net volume flux evolves over time, within a period,for the two front edges and the reference solution. The blue hatched areas indicate the values each quantity can reach based on the standard deviation ($\mu_Q \pm 3\sigma_Q$). The solution corresponding to max. F_2, has noticeable backflow, which makes the net volume flux to be negative for a great part of the period (a bit less than half of the period). However, the positive overweighs the negative part resulting in max. F_2. This appears to be a quite unstable solution, as it is seriously affected by the uncertainties of the design variables.Regardingthemin. F_1solution, with the selected resolution in time (20 steps within a period), the backflow becomes negative during a single step, in which case the instantaneous net volume flux remains positive. In contrast, the reference solution has much greater backflow compared even to the max. F_2 solution. The net volume flux is positive during half of the period and negative during the rest of it,yielding a smaller Q_{net} than the ever computed maximum. From this point of view, any of the Pareto solutions by far outperforms the reference pump.

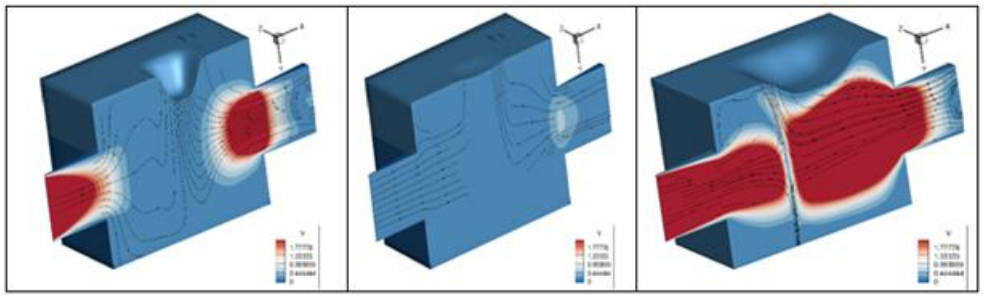

Figure ***6*** shows the flow field of the two front edges and the reference solutions. It can be seen that the reference solutions; the reference solution has instantaneously the highest backflow compared to the other solutions.

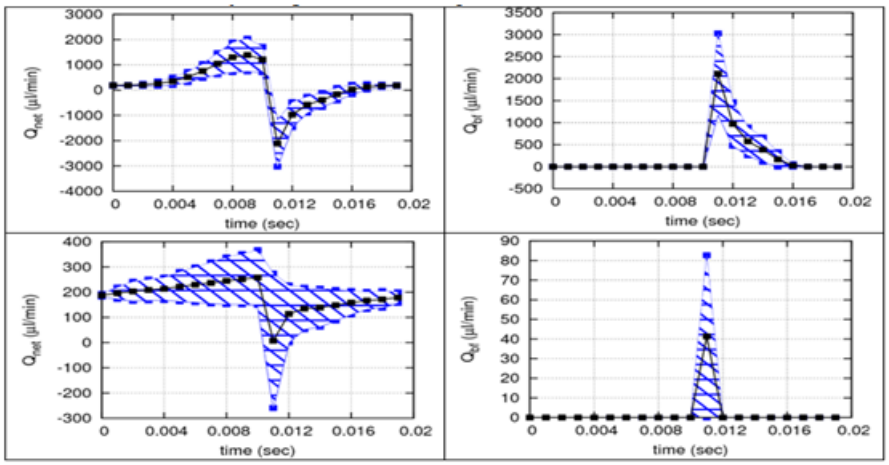

Figure 5$Q_{net}$and Q_{bf} times-series for the max. F_2 (top), min. F_1 (middle) and the reference (bottom) solutions taken from the Pareto front.Mean time-distributions are plotted with a black line and black filled points; the hatched area signifies the zone between $\mu - 3\sigma$ and $\mu + 3\sigma$. Note the different scaling in the vertical axis.

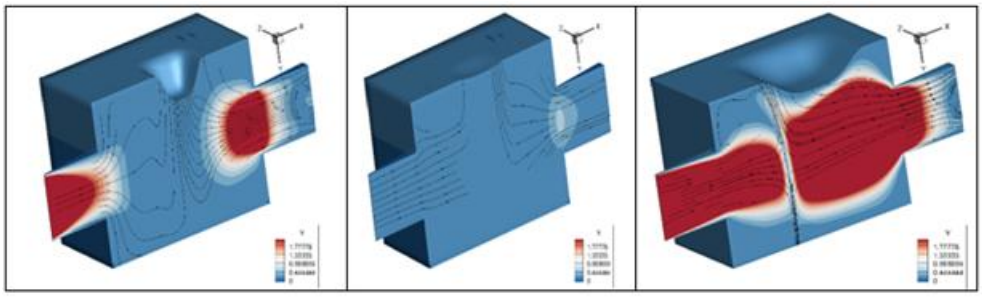

Figure 6 *Instantaneous (at the same instant, the one in which the reference pump has the greatest backflow.) velocity magnitude fields for the max.* F_2*, min.* F_1 *andreferencediaphragm'smotions.Yaxisnotinscale.*

VII. CONCLUSIONS

Thepurpose of this paper was to (a) present a design-optimization workflow and (b) apply it for the redesign of a valveless diaphragm micropump for medical applications, by considering uncertainties associated with the design variables. In contrast to a previous work by the authors, on the same micropump, these operational of manufacturing uncertainties are used during the optimization by formulating and optimizing objective functions combining the mean values and standard deviations of the performance metrics. The background optimization tool is an EA, assisted by RBF networks trained on the fly, separately for each and every new candidate solution, and the processing of each population using PCA. This is hybridized with a gradient-based refinement of some of the current optimal solutions. To compute the gradient of the objective function(s), the continuous adjoint method was mathematically formulated, programmed and used. Regarding uncertainties, the non-intrusive variant of the PCE and a Smolyak sparse grid were used. Using the above s/w, the Pareto front of the optimal solutions was computed with the net flowrate and the backflow as quality metrics.

ACKNOWLEDGMENT

We acknowledge support of this work by the project "Design-Optimization of Diaphragm Pumps under Operational/Manufacturing Uncertainties using the Cut-Cell Method and Polynomial Chaos Expansion" (MIS 5004541) which is implemented under the Action "Supporting Researchers with an Emphasis on Young Researchers", in the context of the call EDBM34, funded by the Operational Programme "Human Resource Development, Education and Lifelong Learning" (NSRF 2014-2020) and co-financed by Greece and the European Union (European Regional Development Fund).

REFERENCE

[1]. P. Dhananchezhiyan and S. Hiremath. Optimization of multiple micro pumps to maximize the flow rate and minimize the flow pulsation. Procedia Technology, 25:1226-1233, 2016.
[2]. E. Stemme and G. Stemme. A valvelessdifuser/nozzle-based fluid pump. Sensors and Actuators A: Physical, 39:159–168, 1993.
[3]. M. Eldred and J. Burkardt. Comparison of non-intrusive Polynomial Chaos and stochastic collocation methods for uncertainty quantification. In American Institute of Aeronautics and Astronautics, 2009.
[4]. D. Kapsoulis, K. Samouchos, X. Trompoukis, and K. Giannakoglou. Hybrid optimization of a valveless diaphragm micropump using the cut-cell method. Journal of Mechanics Engineering and Automation, to be published, 2019.
[5]. D. Kapsoulis, K. Tsiakas, X. Trompoukis, V. Asouti, and K. Giannakoglou. A PCA assisted hybrid algorithm combining EAs and adjoint methods for CFD-based optimization. Applied Soft Computing, 73:520-529, 2018.
[6]. M. Karakasis and K. Giannakoglou. On the use of metamodel-assisted, multiobjective evolutionary algorithms. Engineering Optimization, 38(8):941-957, 2006.
[7]. A. Nisar, N.Afzulpurkar, B.Mahaisavariya, and A. Tuantranont. MEMs-based micropumps in drug delivery and biomedical applications. 2008.
[8]. K. Samouchos, S.Katsanoulis and K. Giannakoglou. Unsteady adjoint to the cut-cell method using mesh adaptation on GPUs. In Presented at the ECCOMAS Congress, Crete Island, Greece, 2016.
[9]. K. Samouchos, D. Kapsoulis, X. Trompoukis and K. Giannakoglou. Shape optimization of 3D diaphragm pumps using the continuous adjoint approach to the cut-cell method. In Presented at the ICCM Congress, Singapore, 2019.
[10]. K.Sindhya, K. Miettinen, and K. Deb. A hybrid framework for evolutionary multi-objective optimization. IEEE Transactions on Evolutionary Computation, 17:495-511, 2013.
[11]. S. Smolyak. Quadrature and interpolation formulas for tensor products of certain classes of functions. Dokl. Akad. Nauk SSSR., 4:240-243, 1963.
[12]. D. Xiu and G. Karniadakis. The Wiener-Askey polynomial chaos for stochastic differential equations. Arch. Comput. Methods Eng., 24(2):619-644, 2002.
[13]. Y. Bar-Cohen and Z. Chang. Piezoelectrically actuated miniature peristaltic pump. Proceedings of SPIE's 7th Annual International Symposium on Smart Structures and Materials, 39:92-103, 2000.

D. Kapsoulis" Optimization under Uncertainties of a Valveless Diaphragm Pump using the Cut-Cell Method" The International Journal of Engineering and Science (IJES), 8.8 (2019): 07-14